

The Effects of Surface Roughness Length, Translational Velocity, and Swirl Ratio on an Idealized Tornado

MARTIN SATRIO

*Advanced Radar Research Center, Norman, Oklahoma
School of Meteorology, Norman, Oklahoma*

DAVID BODINE

Advanced Radar Research Center, Norman, Oklahoma

ANTHONY REINHART

*Cooperative Institute for Mesoscale Meteorological Studies, Norman, Oklahoma
National Severe Storms Laboratory, Norman, Oklahoma*

T. MARUYAMA

Kyoto University, Kyoto, Japan

1. Introduction

Tornado structure is known to be sensitive to the characteristics of near-surface inflow (Lewellen et al. 1997, 2000) which can be altered by the translational velocity of the tornado as well as the characteristic surface roughness length. Many observational studies such as Forbes 1998 and the VORTEX-SE project have identified potential influences of surface terrain on tornado dynamics, particularly in areas of complex terrain such as the southeast United States. However, these effects are difficult to study observationally due to temporal and spatial limitations of observations. For instance, though current mobile Doppler radars have the ability to provide full-volume scans every 20 seconds, there remains considerable limitations on tornado research conducted through such methods. Such limitations include large errors in three-dimensional wind retrievals from single or dual-Doppler analyses and inability to observe in the lowest levels where strong inflow exists (Dowell et al. 2005; Bodine et al. 2016b). Consequently, tornado data acquired from Doppler radar is most useful when supplemented with knowledge obtained about tornado flow structure from idealized simulations.

Previous experiments attempting to dissect properties of tornado flow structure include the Ward Chamber (Ward 1972; Church et al. 1977, 1979), where it was found that certain characteristics of the flow were dependent mostly on the swirl ratio, S , with a weaker dependence on the Reynolds number, Re_F . More specifically, as S increased, the tornado transitioned from a single vortex containing all updraft, to a single vortex with an axial

downdraft above the surface, to a two-celled vortex, and finally to a multiple-vortex tornado. Extended research was conducted with the Fiedler Chamber (Fiedler 1995) with flow dependent also on a different swirl ratio, Ω , and the Reynolds number, Re_F . Many numerical simulations have followed the Fiedler model using different values for Ω and Re_F (Fiedler 1994, 1998, 2009; Nolan and Farrell 1999; Nolan 2005). The main motivation of this study stems from Lewellen et al. (1997, 2000) who utilized a large-eddy simulation (LES) model to simulate an idealized tornado and likewise determined that the tornado flow was dependent on the swirl ratio and Reynolds number. Additionally, the authors also concluded that there are other variables related to near-surface characteristics including surface roughness, translational velocity, and inflow velocity profiles which in turn affect tornado behavior. For example, Lewellen et al. (1997) concluded that an increase in translational velocity from 0 m s^{-1} to 15 m s^{-1} resulted in an increase in the maximum mean velocity by 5 m s^{-1} , as well as a one-third increase in the maximum velocity variance. The vortex also becomes less vertically aligned, with the lower section of the tornado lagging behind and to the right of the center of the domain.

While the surface roughness length and translational velocity affect tornado structure, a comprehensive sensitivity study of this parameter space has yet to be done. The goal of the current study is to provide a comprehensive sensitivity study of the impact of surface roughness and translational velocity to understand how these factors impact tornado dynamics. To accomplish this, a large-eddy simula-

tion (LES) model is used to simulate an idealized tornado moving at different speeds and over surfaces of different roughness. Different boundary conditions are also applied to create a low, medium and high swirl base flow to understand how representative these changes are across a spectrum of tornado flow.

2. Methods

The LES model utilized in this study stems from the Research Institute for Applied Mechanics Computational Prediction of Airflow over Complex Terrain (RIAM-COMPACT) model (Uchida and Ohya 2003; Maruyama 2011) at Kyushu University. The LES has a domain of $1 \text{ km} \times 1 \text{ km} \times 2 \text{ km}$ which utilizes a stretched grid with 176, 176, and 80 grid points in the x , y , and z directions, respectively. The finest horizontal resolution is approximately 3 m in the center of the domain and the finest vertical resolution is approximately 3.7 m at the bottom of the domain. Thus, the domain is large enough to encompass the strongest velocities within the tornado while the grid spacing is fine enough at the lower-levels near the center of the tornado to capture the turbulent structures that dominate in that region. However, since the domain is not large enough to capture the parent storm, all flow in the LES is dynamically forced through boundary conditions designed to mimic typical flow that would exist outside of the domain. The horizontal boundaries implement approximately axisymmetric flow in the inflow region through a depth of 200 m. Above this inflow layer, the radial velocities are held at 0 m s^{-1} with angular momentum being held constant. The top boundary conditions induce an updraft with an average velocity of 19 m s^{-1} in a 500 m radius from the center of the domain. The top boundary conditions are governed by the following equations:

$$w(r) = \begin{cases} 44.8 \frac{r}{0.4l_{dom}} - 20 & r \leq 0.4l_{dom} \\ 24.8 & r > 0.4l_{dom} \end{cases} \quad (1)$$

The translational velocity of the tornado is implemented by a moving boundary at the surface while surface roughness is implemented using a logarithmic law for surface stress at a specific roughness length. The surface stress on the first grid point is governed by

$$u_* = \frac{V_H(z_1)\kappa}{\log\left(\frac{z_1}{z_0}\right)} \quad (2)$$

$$\tau = \rho u_*^2 \quad (3)$$

where u_* is the friction velocity, V_H is the horizontal wind speed, and κ is the Von Kármán's constant. (see Bodine et al. (2016a) for supplementary information on the boundary conditions and grid design of the LES model). Variables such as tangential velocity, radial velocity, and pressure are quantified at multiple heights to analyze the

differences in tornado structure and intensity for several different combinations of translational velocities and surface roughness lengths. For each simulation, the vortex was allowed a spin-up time to reach a quasi-steady state. The total analysis time was approximately 200 s with a temporal resolution of approximately 1.2 s. A high-temporal resolution case with Δt of 0.5 s was also run for some of the simulations to analyze subvortices within the tornado. The translational velocity of the tornado is varied from 0 m s^{-1} , to 10 m s^{-1} , and then to 20 m s^{-1} . The surface roughness length is varied from 0.001 m, 0.01 m, 0.1 m, and 1 m. A surface roughness of 0.001 m physically represent a very smooth, almost water-like surface, 0.01 m represents a smooth pasture, 0.1 m represents a rougher field with sparse vegetation, and 1 m represents a suburb or forest.

3. Results

a. Swirl Ratio and Surface Roughness

Figure 1a and 1b show the time-averaged cross-section through the direction of motion for the low and medium swirl cases for a surface roughness length of 0.1 m, respectively. The high swirl case is not shown as its characteristics closely resemble that of a medium swirl case with a wider core. The idealized tornado in the low swirl case is much narrower than the medium swirl case, and represents a one-cell vortex through the depth of the domain. The tornado in the medium swirl case is an end-wall vortex that erupts into a two-cell vortex aloft. Additionally, and perhaps more importantly, the medium swirl case exhibits vortex breakdown into multiple subvortices rotating around the main circulation while the low swirl does not. The subvortices will be analyzed in further detail later on. Another distinct difference between the two swirl ratio cases is in the corner flow region, namely, the low swirl case lacks the radial outflow in the corner flow region while the medium swirl case clearly exhibits the in-up-out motion as shown by the arrows.

Figure 2 shows the maximum tangential velocity, minimum radial velocity, maximum vertical velocity, and maximum pressure deficit profiles in the lowest 100 m for both swirl cases a surface roughness length of 0.001 and 0.1 m. For a surface roughness length of 0.001 m, the low swirl tornado has a higher maximum tangential velocity through the lowest 100 m, while for a surface roughness length of 0.1 m, the opposite is true. In the lowest 20 m, the maximum tangential velocity for both the low and medium swirl cases are both significantly decreased by the effects of friction as surface roughness is increased. However, for the medium swirl case, maximum tangential velocities occur at around $z=40 \text{ m}$ for the higher surface roughness case. For the low swirl case, this overshoot never occurs, resulting in lower tangential velocities throughout the lowest 100 m for the $z_0=0.1 \text{ m}$ simulation.

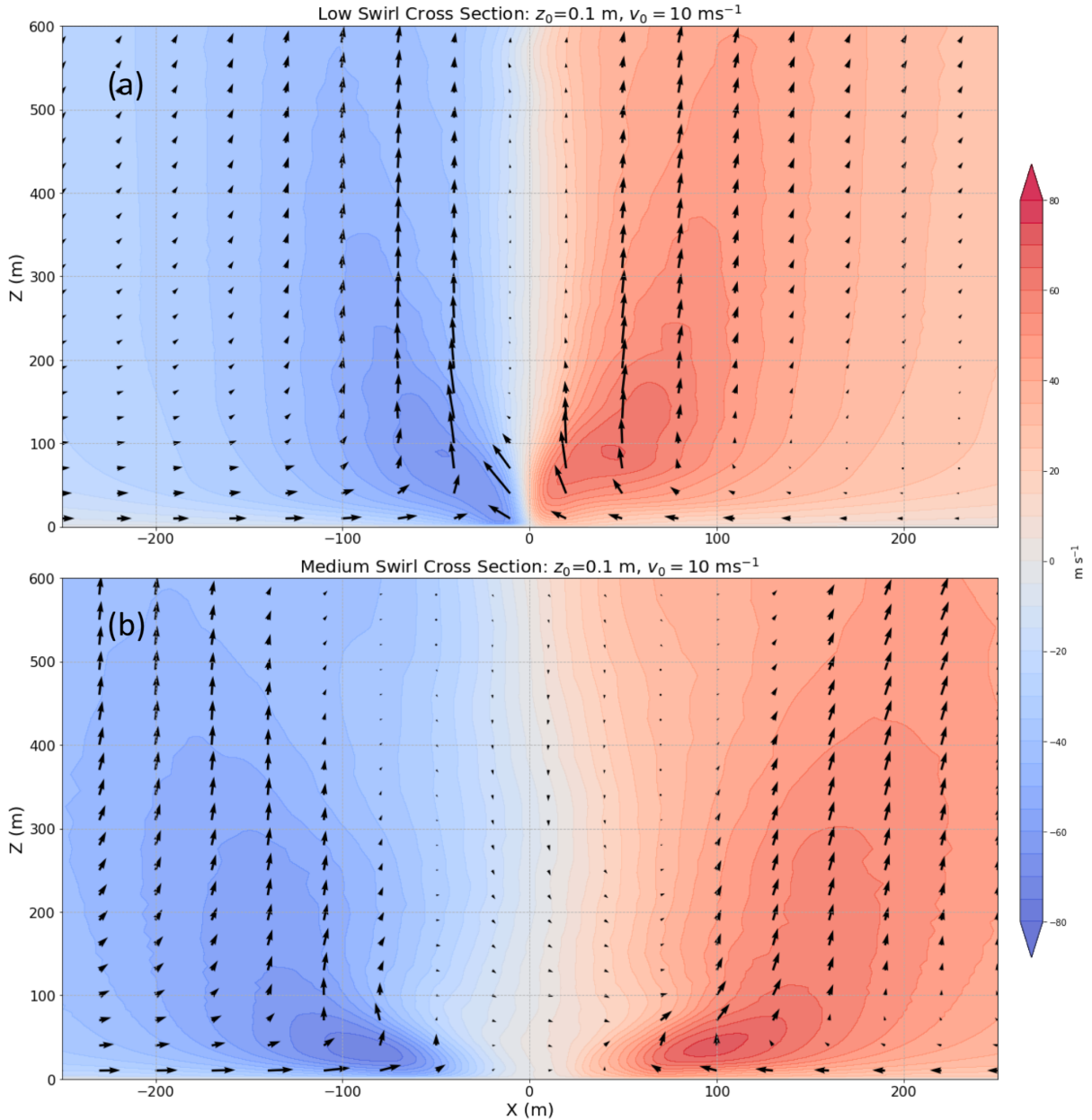


FIG. 1. Time-averaged left-right cross section with a surface roughness length of 0.1 m and translational velocity of 10 m s^{-1} for (a) the low-swirl case and (b) the high-swirl case (top right).

Looking at the minimum radial velocity profiles, the maximum inflow for all four simulations are found near 10 m AGL. For both the medium and low swirl cases, an increase in the surface roughness corresponds to an increase in the maximum inflow due to the effects of friction. Additionally, the inflow in the medium swirl cases for both surface roughness lengths is greater than in the low swirl case. The opposite is true for vertical velocity: the maximum vertical velocity profile for the lowest

100 m in the low swirl case is significantly greater than in the high swirl case. While for the medium swirl case an increase in the surface roughness length does not significantly change the vertical velocity profile, an increase in friction acts to increase vertical velocities in the lowest 100 m. Lastly, the pressure deficit for the low swirl case is substantially greater than the medium swirl case for both surface roughness lengths. Moreover, while an increase in friction acts to very slightly increase the pres-

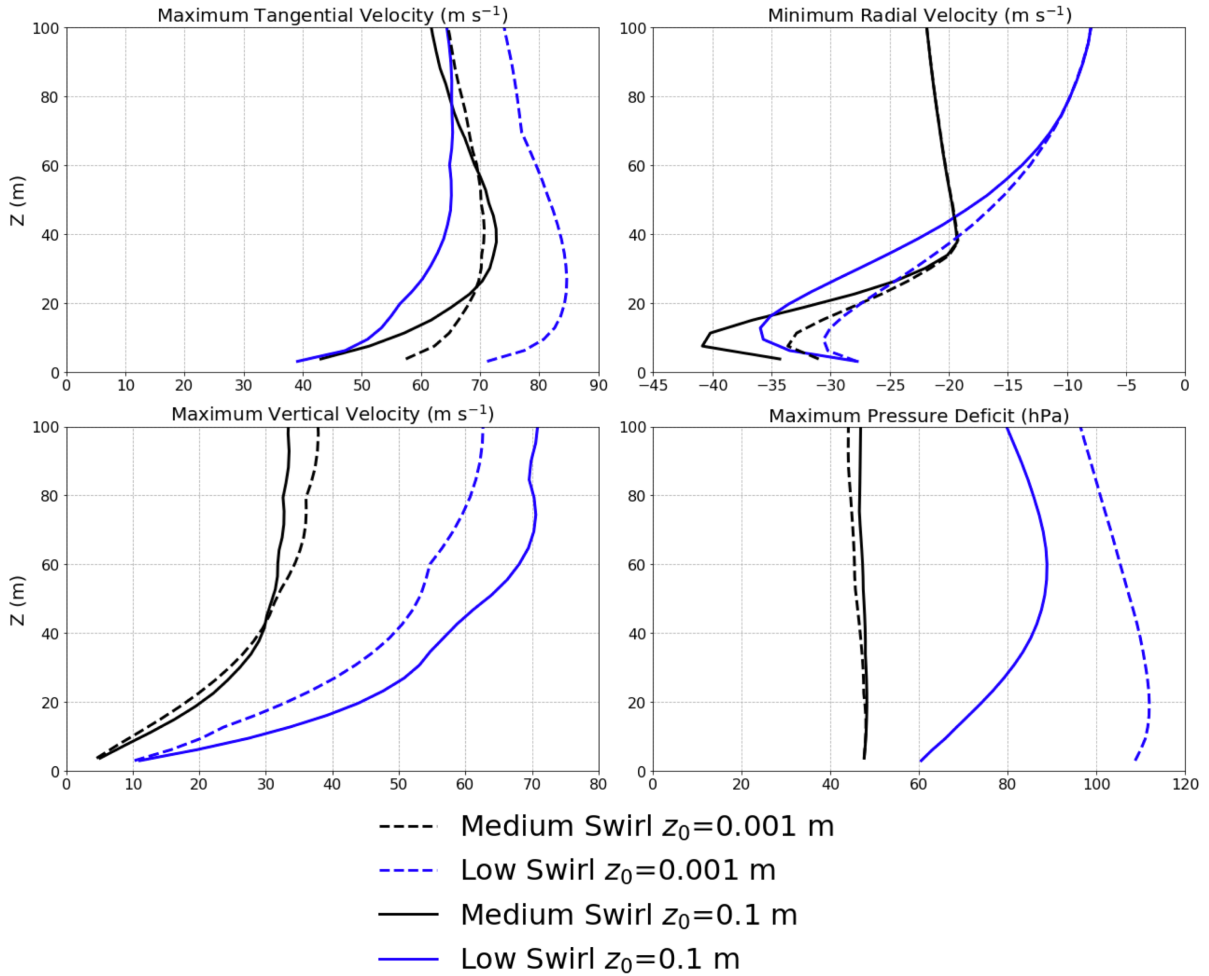


FIG. 2. Profiles in the lowest 100 m of maximum tangential velocity, minimum radial velocity, maximum vertical velocity, and maximum pressure deficit for the low swirl (blue) versus medium swirl (black) and $z_0 = 0.001$ m (dashed) versus $z_0 = 0.1$ m (solid).

sure deficit for the medium swirl case, the low swirl case exhibits a drastic decrease in the pressure deficit with an increase in friction. Overall, near-surface profiles for the low swirl case seems to be affected more by a change in surface roughness length as compared to the medium swirl case. This is especially apparent when looking at the profiles of tangential velocity and pressure deficit, but is also evident in the radial velocity profile.

b. Radar Averaging

Though the LES model's high temporal and spatial resolution has the capability to fully resolve subvortices within the tornado, one of the questions this study seeks to address is the characteristics of the tornado that a radar would resolve, including whether or not these subvortices can be detected radars. Figure 3 averages the v -component

of the wind horizontally and vertically at a height of approximately 34 m using grid spacing of 12 m, 50 m, 100 m and 250 m designed to represent radar resolutions from different wavelengths from W-band to S-band. The actual v -component of the wind at 34 m AGL is overlaid and labeled with black contours. Note that although the averaging does not consider the geometry of the radar scans (such as a widening beam width, beam tilting with range, etc.), the figure roughly represents what the radar scan would look like if the tornado was located just north of the radar. Also note averaging is done only spatially, not temporally.

From Figure 3, the purple circles mark the location of some of the subvortices that are rotating around the main tornado, indicated by tight gradients in v . The radar images for all resolutions are dominated by $v > 0$ to the right of the tornado and $v < 0$ to the left of the tornado as expected. In terms of subvortices, even at the highest reso-

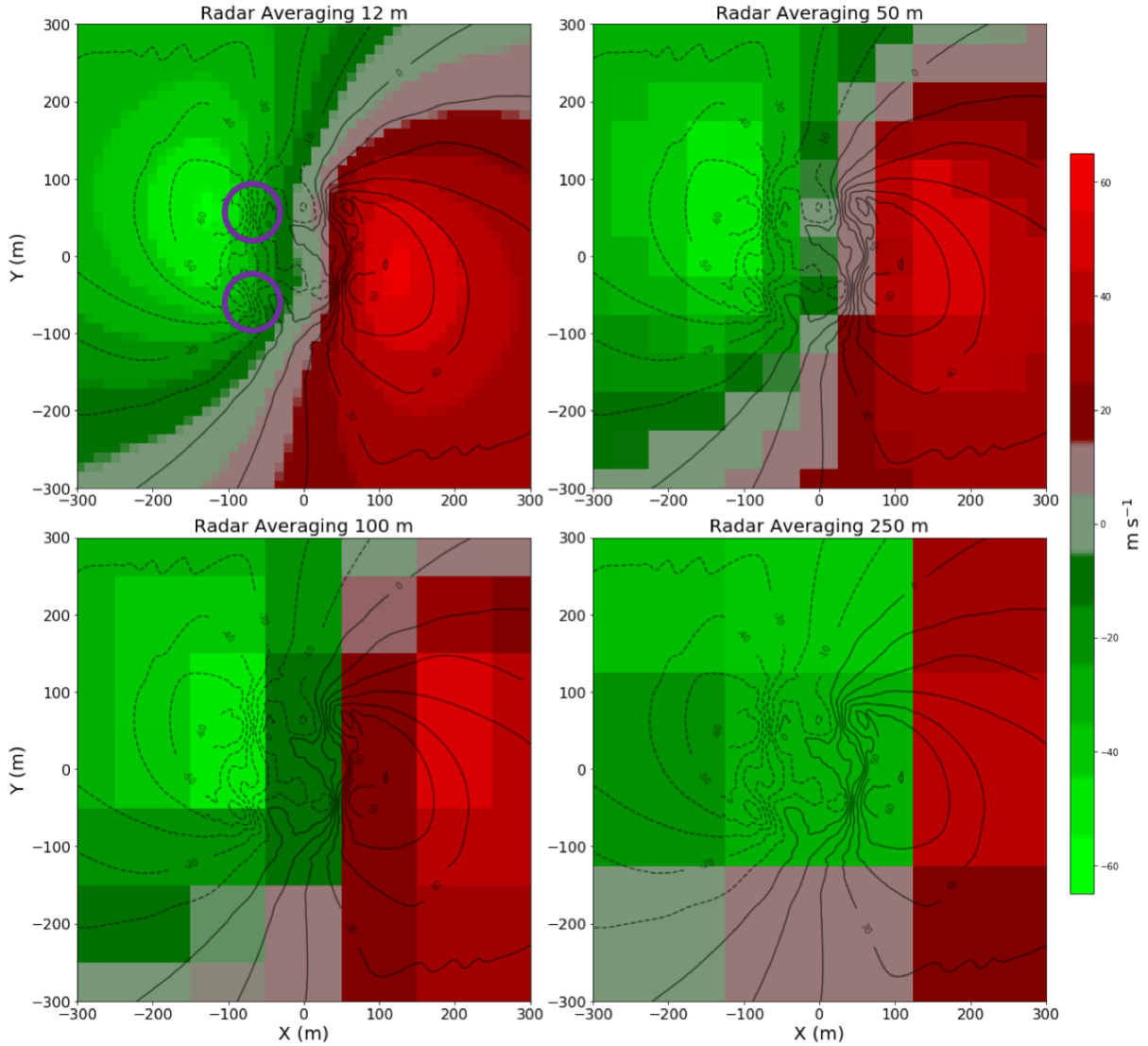


FIG. 3. Horizontal and vertical spatial averaging of the LES model at a height of 34 m using grid spacing of 12 m (top left), 50 m (top right), 100 m (bottom left), and 250 m (bottom right) in order to simulate a radar image. The actual v-component of the wind is contoured in black. The purple circles in the top left plot denotes two locations of subvortices.

lution of 12 m, it is impossible to determine the location of any of the subvortices, let alone characteristics of the subvortices such as strength and size. Simply put, the subvortices are averaged out. The next method to try to extract any information about the subvortices was to take different between radar scans at two different elevations. The radar scan at 30 m at a particular resolution was subtracted from the radar scan at approximately 200 m where subvortices were not dominant, with the goal of weeding out differences due to subvortices. Though not shown, the difference plots between two elevations showed no success in highlighting characteristics or locations of the subvortices.

Lastly, ΔV for each of the time steps in each of the simulations was recorded in order to give a time-series plot for ΔV . Though not shown, the actual ΔV has much more fluctuations than the ΔV recorded by radar, owing to the inability of the radar to resolve small scale fluctuations in V with the subvortices. The radar also underestimates the actual ΔV by approximately 30 m s^{-1} for 12 m resolution, 40 m s^{-1} for 50 m resolution, and 50 m s^{-1} for 100 m resolution, again since the most extreme velocities are being averaged out. However, the radar scan is capable of following the general pattern of ΔV . A 250 m resolution underestimated by as much as 80 m s^{-1} .

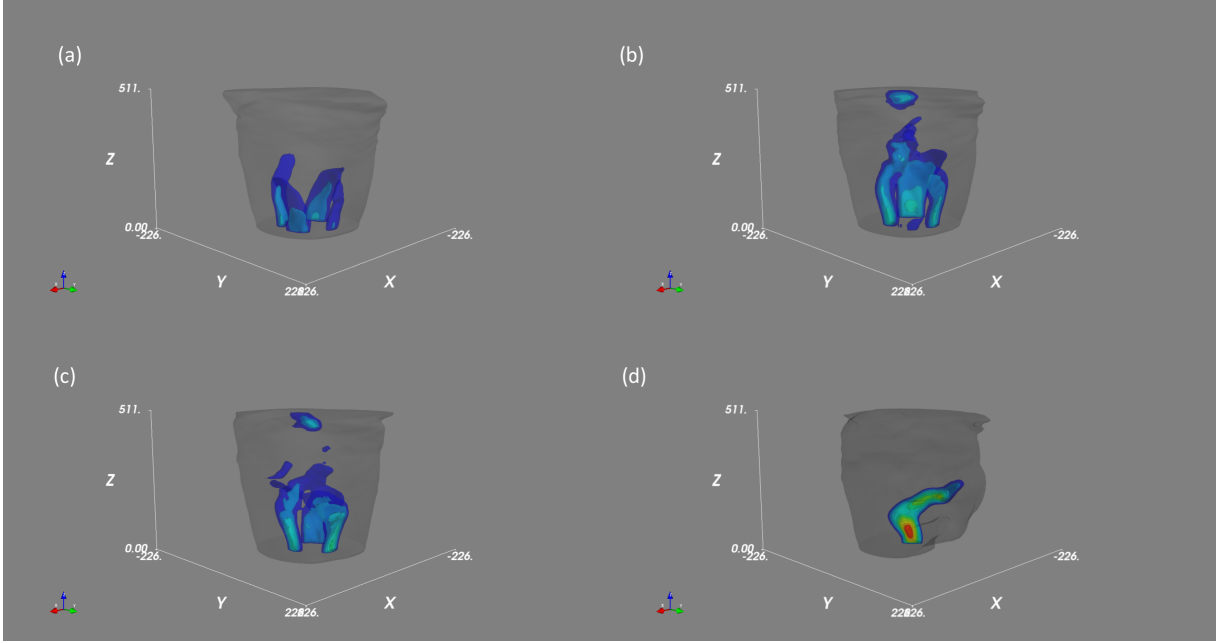


FIG. 4. Snapshots of subvortex structure for (a) $z_0 = 0.001$ m, (b) 0.01 m, (c) 0.1 m and (d) 1 m with $v_0 = 10$ m s⁻¹ about 65 seconds into the analysis time. The outer gray contour represents a pressure deficit of 25 hPa. The first colored (dark blue) contour represents a pressure deficit of 50 hPa and each contour is 5 hPa thereafter.

c. Effects of Varying Surface Roughness on Subvortices

One of the most striking differences between the LES simulations of different surface roughness lengths is the behavior and characteristics of the subvortices. Figure 4 shows a 3-dimensional snapshot of the subvortices using pressure deficit surfaces. The size, strength, shape, and number of subvortices rotating around the main circulation differ drastically with changing surface roughness length. One of the goals of the project is to track these subvortices through time at different heights, recording characteristics such as the wind field, pressure, etc. for a more in-depth analysis. The algorithm developed to track the subvortices utilized the second derivative of the pressure field in order to find the maximum of the pressure deficit. Figure 5 shows a surface plot of the negative second derivative of the pressure anomaly field, with the peaks representing location of subvortices. The location along with variables such as maximum horizontal wind, maximum vertical wind, and minimum pressure in a 20 m radius around the center location of the subvortex are recorded. Figure 4b shows the percentage that a particular number of subvortices exists for each of the surface roughness cases. For the lowest surface roughness length, 0.001 m, the simulation has 4 to 5 subvortices throughout the analysis time, with a some times having up to 6. The 0.01 m case has 4 to 5 subvortices the 0.1 m has 3 to 4 subvortices, and the 1 m case has 1 to 2 subvortices.

Further analysis is done by representing each of the subvortices as objects, such that characteristics of each individual subvortex can be obtained. The method for obtaining the subvortices through time and space are as follows.

- (i) For a subvortex to exist, there must be a point detected at the lowest grid point from the previous algorithm using the second derivative of the pressure deficit field
- (ii) Once the surface center point is detected, the closest point that is less than 25 m away at the next grid point is chosen. If such a point does not exist, the subvortex ends at that height. If the subvortex does not extend to at least 3 elevations up from the surface (11.3 m), then it is not classified as a subvortex. After this step is completed, each analysis time will have the data for the separate subvortices.
- (iii) The next step is to match up the subvortices from a previous analysis time, $t_i - 1$ to the subsequent time t_i , i.e. does the subvortex at a particular analysis time match up with one from a previous time, or is it a new one? Take a subvortex at $t_i - 1$ and define new guess subvortex location given by

$$x_{search} = x_{t_i-1} - 30\sin(\tan^{-1}(\frac{y_{t_i-1}}{x_{t_i-1}})) \quad (4)$$

$$y_{search} = y_{t_i-1} + 30\cos(\tan^{-1}(\frac{y_{t_i-1}}{x_{t_i-1}})) \quad (5)$$

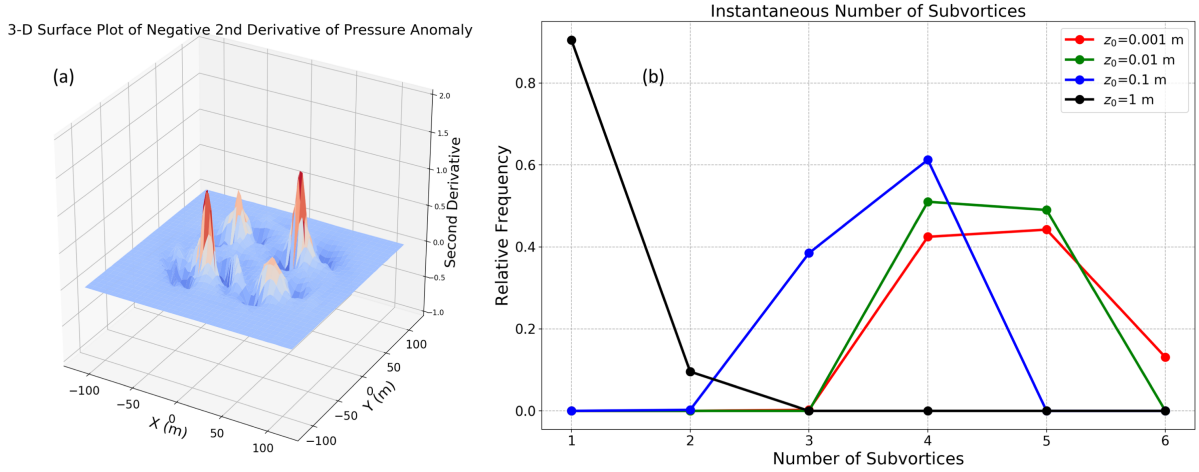


FIG. 5. (a) A 3-dimensional surface plot of the negative of the second derivative of the pressure deficit field and (b) plot indicating the percentage of time that a particular number of subvortices exists for the case with $z_0 = 0.001$ m (red), 0.01 m (green), 0.1 m (blue), and 1 m (black) with $v_0 = 10 \text{ m s}^{-1}$

- (iv) If at t_i there is a subvortex within 30 m of x_{search} and y_{search} , then that subvortex is matched with the old one. If there is no subvortex within 30 m, then the subvortex is said to have dissipated. If there is more than one subvortex within the defined area, the closest one is chosen.
- (v) Once all subvortices at $t_i - 1$ have been accounted for, if there are any subvortices at t_i that have not been matched with an old one, it is registered as a new subvortex.

From the analysis, it seems like there are two fairly distinct categories; long-lived subvortices and short-lived subvortices. We define a short-lived subvortex to be lasting no longer than 5 s. The data for the long-lived subvortices is then averaged to get a good idea of the subvortex characteristics for each surface roughness case, summarized in Table 1. An interesting find is that the subvortices in the 0.01 m surface roughness case is much more stable than the other cases. The 0.001, 0.1, and 1 m case each have 18, 14, and 7 subvortices with only 1 subvortex in the 0.1 m case lasting the entire analysis time of about 204 s. Meanwhile, in the 0.01 m case, there are only 5 different subvortices. Additionally, the 4 subvortices that exist at the start of the analysis time never dissipate, and there is one subvortex that forms in the middle of the analysis time and has a lifetime of 100 s, or about half the analysis period. Further analysis into the dynamical reasons why the 0.01 m case favors much more stable subvortices should be conducted for future work.

Further inspection into the characteristics of the subvortices reveal that the translational speed for the long-lived subvortices decreases with increasing surface roughness.

While the subvortices in the 0.001 m case travel at an average speed of about 40 m s^{-1} , there is a small decrease of speed in the 0.01 m case, followed by a sharper decrease to 37 m s^{-1} in the 0.1 m case and an even sharper drop to 26.6 m s^{-1} for the 1 m case. The average distance of the long-lived subvortices from the center of the domain also decreases with increasing surface roughness, with an average distance of about 55 m in the lowest surface roughness case down to 27 m for the highest surface roughness case. This is coincident with a constriction of the corner flow region towards the axis of rotation for higher surface roughness lengths. Additionally, the time-averaged maximum vertical velocity as well as the maximum pressure deficit increases with surface roughness.

4. Conclusions

This study utilizes an LES model to examine the effects of varying swirl ratio and surface roughness lengths on the structure and dynamics of the tornado. It is found that while the low swirl tornado resembles a one-cell vortex throughout the depth of the domain, the medium swirl case is characterized by an end-wall vortex at the surface which transitions to a two-cell vortex aloft. While both the low swirl and medium swirl case are affected by varying surface roughness, it is evident that an increase in friction has a greater impact on the mean wind components for the low swirl case. The medium swirl case also undergoes vortex breakdown leading to the formation of secondary vortices that rotate around the main circulation. Using spatial averaging, a pseudo radar image can be created to assess the characteristic of the idealized tornado that a radar would be able to resolve. Although the radar is able to resolve

TABLE 1. Characteristics of the long-lived (>5 s) subvortices for each of the surface roughnesses. Columns from left to right represent surface roughness, the lifetime or duration, translational speed, distance from the center of domain, time-averaged maximum horizontal velocity, time-averaged maximum vertical velocity, and time-averaged maximum pressure deficit.

z_0 (m)	No. of Subvortices	Time-Avg Duration (s)	Time-Avg Speed (m s^{-1})	R (m)	Max uv (m s^{-1})	Max w (m s^{-1})	Min p (hPa)
0.001	18	105.0	40.3	55.4	107.2	61.0	83.0
0.01	5	183.3	39.8	52.2	109.78	66.7	85.1
0.1	14	104.0	36.9	45.4	104.85	69.9	84.5
1.0	7	53.83	26.6	27.12	104.5	80.8	116.0

the overall pattern of the flow, it would be unable to capture any details regarding the subvortices. Additionally, since the radar cannot resolve small scale fluctuations in the horizontal wind within the subvortices, the radar underestimates ΔV by about 30 m s^{-1} for a 12 m horizontal resolution up to 80 m s^{-1} for a 250 m (S-band) resolution.

Lastly, a more detailed analysis focusing on just the subvortices is done for the tornado translating at 10 m s^{-1} . Using a tracking algorithm, the number of subvortices in a simulation is found to decrease as the surface roughness increases: the 0.001 m case has 4-6 subvortices, the 0.01 m has 4-5 subvortices, the 0.1 m case has 3-4 subvortices, and the 1 m case has 1-2 subvortices. The stability of the individual subvortices also seems to be affected by changes in surface roughness. In particular, subvortices within the 0.01 m case are much more stable compared to the others, with only 5 different subvortices the whole analysis period and 4 of those 5 never dissipating during the whole simulation. Meanwhile, the subvortices in the other simulations are much more erratic, with a clear distinction between long-lived and short-lived subvortices. Calculating averages from the long-lived subvortices, it is concluded that with increasing surface roughness, the distance from the center of rotation decreases, the translational speed of the subvortices decreases, and the time-averaged maximum vertical velocity as well as the maximum pressure deficit increases.

For future work, the analysis will be repeated for a set of varying translational velocities. Furthermore, additional analyses into why subvortex behavior differs between different surface roughness lengths will be conducted. The final goal of the project is to incorporate different terrain such as hills, slopes, buildings, etc. to study how those may affect tornado structure and dynamics. Eventually, simulation of a supercell over realistic terrain such as those found in the southeast United States, where terrain effects are magnified, will be conducted. The data from the simulated supercell will be used as boundary conditions for the LES model.

Acknowledgments. The authors acknowledge support from NOAA grant NA17OAR4590201 (VORTEX-SE) for this work. The authors would also like to thank Takanori

Uchida (Kyushu University) for providing the RIAM-COMPACT LES software.

References

- Bodine, D. J., T. Maruyama, R. D. Palmer, C. J. Fulton, H. B. Bluestein, and D. C. Lewellen, 2016a: Sensitivity of tornado dynamics to soil debris loading. *J. Atmos. Sci.*, **73**, 2783–2801.
- Bodine, D. J., R. D. Palmer, T. Maruyama, C. J. Fulton, Y. Zhu, and B. L. Cheong, 2016b: Simulated frequency dependence of radar observations of tornadoes. *J. Atmos. Oceanic Technol.*, **33**, 1825–1842.
- Church, C. R., J. T. Snow, and E. M. Agee, 1977: Tornado vortex simulation at purdue university. *Bull. Amer. Meteor. Soc.*, **58**, 900–909.
- Church, C. R., J. T. Snow, G. L. Baker, and E. M. Agee, 1979: Characteristics of tornado-like vortices as a function of swirl ratio: A laboratory investigation. *J. Atmos. Sci.*, **36**, 1755–1776.
- Dowell, D. C., C. R. Alexander, J. M. Wurman, and L. J. Wicker, 2005: Centrifuging of hydrometeors and debris in tornadoes: Radar-reflectivity patterns and wind-measurement errors. *Mon. Wea. Rev.*, **133**, 1501–1524.
- Fiedler, B., 2009: Suction vortices and spiral breakdown in numerical simulations of tornado-like vortices. *Atmos. Sci. Letters*, **10**.
- Fiedler, B. H., 1994: The thermodynamic speed limit and its violation in axisymmetric numerical simulations of tornadolike vortices. *Atmos.-Ocean*, **32** (2), 335–359.
- Fiedler, B. H., 1995: On modelling tornadoes in isolation from the parent storm. *Atmos.-Ocean*, **33**, 501–512.
- Fiedler, B. H., 1998: Wind-speed limits in numerically simulated tornadoes with suction vortices. *Quart. J. Roy. Meteor. Soc.*, **124**, 2377–2392.
- Lewellen, D. C., W. S. Lewellen, and J. Xia, 2000: The influence of a local swirl ratio on tornado intensification near the surface. *J. Atmos. Sci.*, **57**, 527–544.
- Lewellen, W. S., D. C. Lewellen, and R. I. Sykes, 1997: Large-eddy simulation of a tornado's interaction with the surface. *J. Atmos. Sci.*, **54**, 581–605.
- Maruyama, T., 2011: Simulation of flying debris using a numerically generated tornado-like vortex. *J. Wind Eng. Ind. Aerodynamics*, **99**, 249–256.
- Nolan, D. S., 2005: A new scaling for tornado-like vortices. *J. Atmos. Sci.*, **62**, 2639–2645.

- Nolan, D. S., and B. F. Farrell, 1999: The structure and dynamics of tornado-like vortices. *J. Atmos. Sci.*, **56**, 2908–2936.
- Uchida, T., and Y. Ohya, 2003: Large-eddy simulation of turbulent airflow over complex terrain. *J. Wind Eng. Ind. Aerodynamics*, **91** (1–2), 219–229.
- Ward, N. B., 1972: The exploration of certain features of tornado dynamics using a laboratory model. *J. Atmos. Sci.*, **29**, 1194–1204.